

Mode detection from line-profile variations

L. Mantegazza

Osservatorio Astronomico di Brera, Merate, Italy
luciano@merate.mi.astro.it

Abstract. The phenomenology associated with line profile variations in δ Scuti stars is reviewed. The three main techniques adopted to detect pulsation modes, i.e., the pixel-by-pixel analysis, the analysis of the moment time series and the Fourier Doppler Imaging are presented and discussed. Their application to the observational data has allowed the reliable detection of several pulsation modes, many of them not detectable with photometric observations. The need of better coordination of simultaneous spectroscopic and photometric campaigns in order to get the complete pulsation spectra of these stars is pointed out. The observation in different campaigns of the same objects has proved that dramatic changes in the mode amplitudes are quite common, even in a couple of years (and maybe less).

In the last part of the paper a recent approach to the mode detection by direct fit of line profile variations in multiperiodic pulsators is described.

1. Historical development

While the presence of radial velocity variations in δ Scuti itself was detected just at the beginning of the century (Wright 1900), the first hints about the possible presence in the same star of line profile variations (hereinafter LPV) were due to Struve about half a century later (Struve 1953).

After a decade of quiescence the studies of the phenomena associated with LPV were resumed by several authors in the mid sixties and seventies. Several different phenomena were announced, such as variable emission in the cores of strong lines, large equivalent width variations and so on (for a review see the paper by Breger 1979). Unfortunately those findings were probably connected to the use of the photographic plate as a detector. As a matter of fact later studies of the same objects performed with photoelectric detectors were not able to confirm any of those findings.

The first reliable observations of LPV in δ Scuti stars were performed at the beginning of the eighties with the advent of the Reticon detector. Several stars were observed by Campos & Smith (1980) and Smith (1982) but unluckily most of them for a few hours in one night only, i.e., while the presence of line profile variations was clearly detected, the data were not sufficient to analyze the variations and to detect periodicities. Generally the few data were phased with the periods available from photometry or radial velocity curves (usually

at that time only one or two periods per star were known). Among the stars studied by these authors only 28 Aql had a sufficient dataset (4 consecutive nights) which allowed the analysis of line width and radial velocity variations. A period-finding program confirmed the presence in both parameters of the two known periods derived from photometry (Smith 1982).

The successive papers showed, beside the changing shape of the line profiles, the presence of moving sub-features in the lines (e.g., Yang & Walker 1986, Walker et al. 1987). In these cases the data were also not adequate for independent period searches, although two attempts were made by Kennelly et al. (1991, 1992), who analyzed 2.5 hours and 5 hours of observations of k^2 Boo and γ Boo, respectively. They did it by sampling at 10 km s^{-1} intervals the intensity residuals in the line profiles derived from the subtraction of the average profile, and computing the Discrete Fourier Transform. Obviously, given the extremely short temporal baseline, the frequency resolution was very poor, allowing only a rough confirmation of the photometric periods.

In the following years it was realized that more intensive campaigns on a few selected objects were more fruitful than sporadic observations of many targets. This was in part the consequence of the photometric studies that were showing that usually many close frequencies were present in the pulsation spectra and consequently longer baselines were needed in order to resolve these frequencies.

Now before discussing in detail the results concerning these campaigns we shall briefly review the phenomenology associated with the LPV, the constraints that it imposes on the observational programmes and the techniques we can adopt to analyze the data.

2. Phenomenology

Fig. 1 shows the LPV observed during one night in the spectrum of BV Cir; in order to clearly show the LPV the average spectrum has been subtracted from each spectrum. We see the presence of waves propagating across the profiles of the lines at 4501, 4508 and 4515 Å from short to long wavelengths, while in the continuum regions there are only noise fluctuations. In the figure the borders of the three lines have been marked by the solid vertical lines.

As we can judge from the figure the typical time-scale for a feature to cross the line is of the order of a few hours, while the amplitudes of these features are of the order of a few thousandths of the continuum intensity.

As is well known we can interpret such variations as the result of the presence of non-radial pulsations: in each zone of the visible stellar disk the pulsation velocity combines with the rotational one and therefore the flux from this zone, because of the Doppler effect, gives a contribution to the line profile at a distance from the line center corresponding to its radial velocity. In this sense, if the pulsation velocity is small with respect to the rotational one, the line profile broadened by rotation supplies a one-dimensional ‘‘Doppler imaging’’ of the stellar disk (Vogt & Penrod 1983). For this reason it is a common practice, when describing the variations across the line profiles, to transform wavelengths into velocities by means of the Doppler formula, assuming the zero velocity at the line center (see, e.g., Fig. 10).

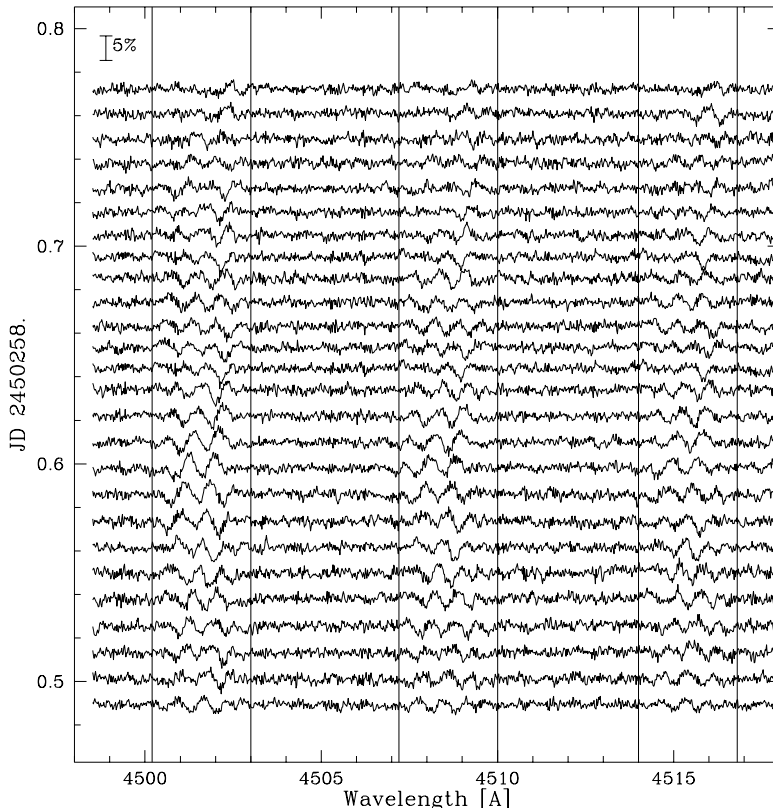


Figure 1. Variations in the line profiles of the lines 4501, 4508 and 4515 Å during one night of observations. The average spectrum has been subtracted to the individual ones in order to better evidence the variations. The small bar at the upper left indicates an amplitude of 5% in the continuum intensity. The vertical solid lines individuate the borders of the three lines. The fluctuations in the continuum regions allow to estimate the S/N which in this case is about 250.

In the case of Fig. 1 the moving features indicate that the prevailing pulsation modes are crossing the visible stellar disk moving in the same direction of rotation (i.e., they are prograde as seen by the observer).

If the set of spectra has a rather good phase coverage of the periods of the different pulsation modes we can get a first guess of some quantities that we need in the further data analysis. First, we can compute the average of the spectra and assume that this approximates the nonpulsation spectrum of the star (however it can be seen that this average spectrum tends to have broader lines than the true nonpulsation one, see, e.g., Hao 1998). Then we can estimate at each wavelength step (or for each pixel of the spectrum) the standard deviation of the normalized flux about the mean.

As an example Fig. 2 shows in the upper panel the average spectrum of X Caeli while the lower panel shows the standard deviation of the individual spec-

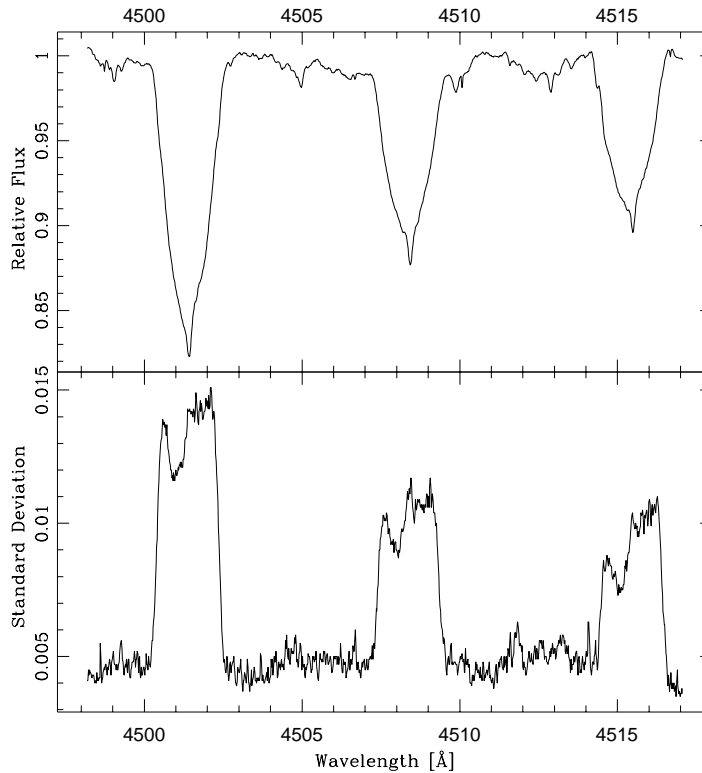


Figure 2. Average spectrum of X Caeli from the data obtained in the 1996 campaign (top panel); standard deviation about the mean of the flux measured in each pixel (bottom panel).

tra about the mean. This panel clearly shows that the variability is restricted inside the line profiles, furthermore it allows the definition for each line of the limits in which the profile variations are present. In the continuum zones the reciprocal of the standard deviation of the normalized fluxes about the continuum supplies an estimate of the S/N of each spectrum, and the reciprocal of the average of the values of the standard deviations of all the spectra about the average one in the same zones gives an estimate of the average S/N at the continuum level. For example in the X Cae case the lower panel of Fig. 2 suggests an average S/N of about 230¹.

Fig. 3 shows the standard deviation of the normalized flux in each pixel for six stars arranged, from the bottom to the top, in order of increasing projected rotational velocity. We can see that as the line profiles broaden the flux variation decreases, until for the fastest rotator ($v \sin i = 196 \text{ km s}^{-1}$) this variation is barely discernible. It can be also appreciated that it becomes increasingly

¹As S/N in Astronomy is usually intended the ratio between amplitudes and not between powers as preferred by engineers.

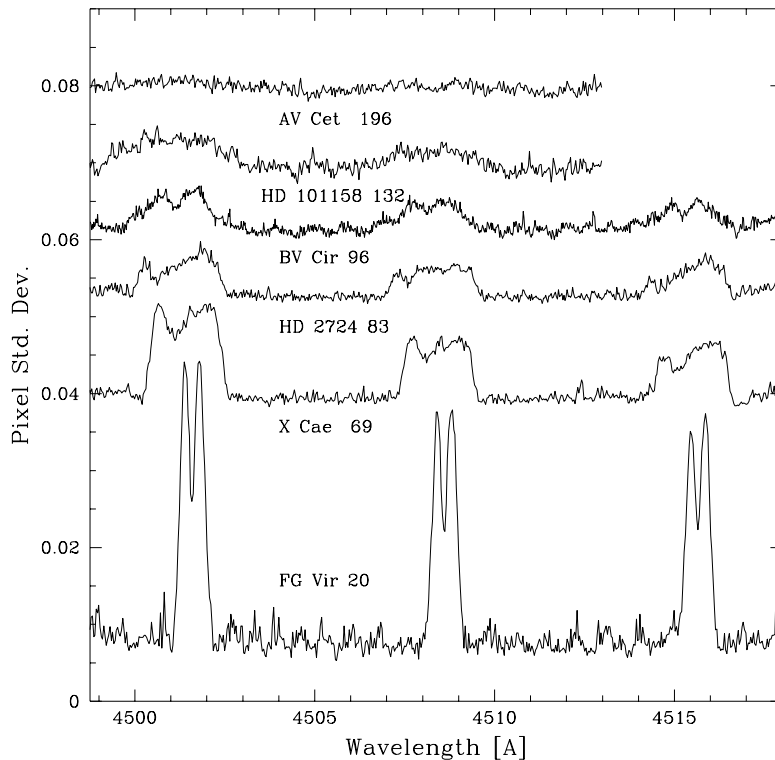


Figure 3. Standard deviations of the normalized flux in each pixel in the same spectral region of six δ Scuti stars. The number beside each star's name is its projected rotational velocity in km/s. The spectra have been vertically shifted to avoid superposition, but the scale is the same.

difficult, as $v \sin i$ increases, to find unblended lines and continuum regions which can be used for the spectrum normalization.

While it is obvious that in order to detect high-degree modes it is necessary to study stars with high $v \sin i$ ², if we consider low-degree modes, it can be shown that in weak lines their S/N ratio decreases approximately with $(v \sin i)^{1/2}$, and therefore these modes are more easily detectable in stars with low projected rotational velocity.

Starting from the average line profile we can also get a first estimate of the projected rotational velocity and of the intrinsic line width. This can be accomplished by performing a non-linear least-squares fit of a rotationally broadened Gaussian profile to the observed one. Fig. 4 shows as an example the fit de-

²As a rule of thumb the highest detectable degree is of the order of $v \sin i / W_i$ (Kennelly et al. 1992), where W_i is the intrinsic line width, i.e., the width that the line should have if rotational broadening was not present.

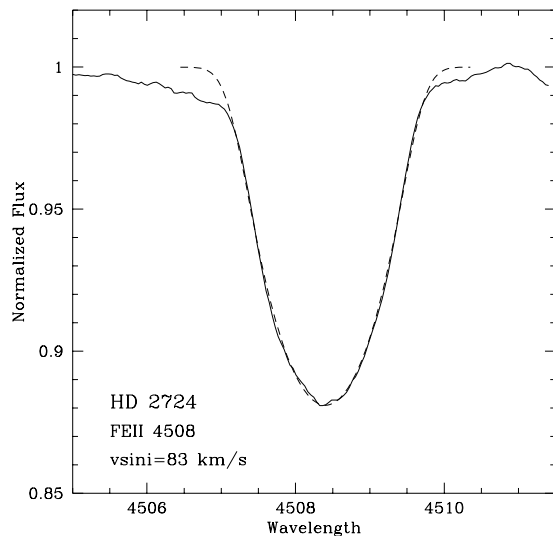


Figure 4. Average profile of the FeII 4508Å line of the star HD2724 (BB Phe) as observed in the 1997 campaign (solid line); rotationally broadened intrinsic profile that best-fit the average one (dashed line). A projected rotational velocity of 83 km s⁻¹ has been derived.

rived in this way on the FeII 4508 Å line of the star HD 2724 (Mantegazza & Poretti 1998). These two quantities can also be estimated using the zero-points of second and fourth moment (Balona 1986b)³. As we have previously said, the average profile tends to be larger than the nonpulsation one. A way to get a better estimate of these two quantities is discussed at the end of this paper.

3. Observational constraints

From what we have shown in the previous section we can estimate what the observational constraints should be in order to detect and to study the LPV in δ Scuti stars.

The typical time-scales of the observed variations (a few hours) impose a limit on the integration times, which should be a fraction of these quantities. According to our experience this limitation is not very stringent for the mode detection, for instance in the case of FG Vir we have detected the 34.1 cd⁻¹ mode with an integration time of 15 min, which corresponds to about 35% of the pulsation period (see Table 1).

For the mode identification the discourse is more delicate, because even if with a relatively long integration time we are still able to detect the fundamental frequency of a mode and to correct its amplitude for the damping due to the integration in time, its harmonics, which are of lesser amplitudes, can be lost

³For the definition of the line moments see the paper by Aerts & Eyer, these proceedings.

in the noise, because of the larger damping due to their shorter periods, and therefore we would not be able to recover the correct shape of the signal.

The amplitudes of the perturbation across the line profiles are for most of the modes of the order of a few thousandths of the continuum intensity, and therefore, to be reliably detected and measured, we need a S/N of at least a few hundred.

Finally, it remains to be evaluated what the minimum spectral resolution should be. Since, as it is explained in the paper by Aerts & Eyer (this proceedings), we can approximate the observed line profiles as the convolution between an intrinsic profile (W_i) and the rotational broadening one, the resolution should be

$$R = \lambda/\delta\lambda \geq c/W_i.$$

Since typically $W_i \simeq 10\text{km/s}$, then $R \geq 30000$.

The three requirements: short exposures, high S/N and high resolution, impose that we collect a lot of photons in short times, and this implies that either we limit ourselves to the study of very bright targets, or we observe with large telescopes, or, by observing a wide spectral region, we find a way to add the information of the LPV contained in many of the observed lines without blurring it.

Up to now 4 different approaches have been adopted to add the information of several lines: a) the straight average of the individual line profiles (e.g., Kennelly et al. 1996); b) the average of the line moments (e.g., Mantegazza & Poretti 1996), c) the computation of the cross-correlation function (e.g., Korzenik et al. 1995), d) the deconvolution of the observed profiles by the intrinsic one (Kennelly et al. 1998, see also the paper by Aerts & Eyer, these proceedings). None of these approaches are free of problems, and in particular all of them assume that the intrinsic profile should be the same for all the lines and therefore in all cases a careful selection of lines with similar characteristics should be done.

4. Analysis techniques

Now we shall briefly review how we can study the variations in a line profile. Three different techniques have been adopted to search for the periodicities present in LPV:

- a) the pixel-by-pixel analysis;
- b) the frequency analysis of the moment time series;
- c) Fourier Doppler imaging.

4.1. Pixel-by-pixel

The pixel-by-pixel analysis is based on the fact that during an oscillation cycle the flux measured in the same pixel of the line profile (i.e., at the same wavelength) fluctuates with the same period. Fig. 5 shows this fact for the TiII 4501 line of the star X Caeli. The profiles have been phased according to the dominant pulsation mode (7.39cd^{-1}) and cover one complete cycle. The dot indicates for each profile the flux at a given fixed wavelength. Therefore we can extract from

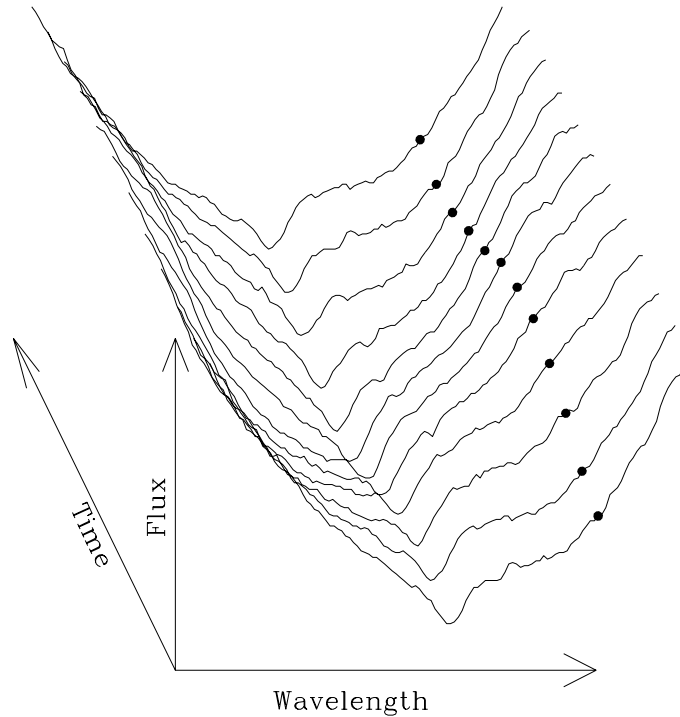


Figure 5. Line profile variations of the 4501Å line in the star X Caeli phased according to its dominant period (7.39cd^{-1}). The dots indicate the flux at a fixed pixel in the line profile.

the set of all the profiles of the same line the time series constituted by the fluxes in the same pixel and then analyze them with the usual techniques developed to study one-dimensional time series (e.g., light-curves). We have seen in the previous section how the diagram showing the flux standard deviation in each pixel can be used to define the line borders and hence to detect which pixels can supply useful time series.

Before extracting the individual pixel time series it is necessary to rebin the spectrograms in order to remove the observer's velocity variations due to the Earth's revolution and rotation. Even the latter cannot be neglected because its amplitude (about 0.5 km s^{-1}) can be comparable to those of the pulsation modes.

Two techniques have been the most frequently used to analyze the pixel-by-pixel time series: a) the least-squares power spectrum (Vaniček 1971), b) the CLEAN algorithm (Roberts et al. 1987)

Fig. 6 shows the application of this approach to analyze the LPV in the FeII 4508 line of BV Cir (1998 campaign, Mantegazza et al. 1999). The upper left panel shows the average line profile, the central panel contains the pixel-by-pixel

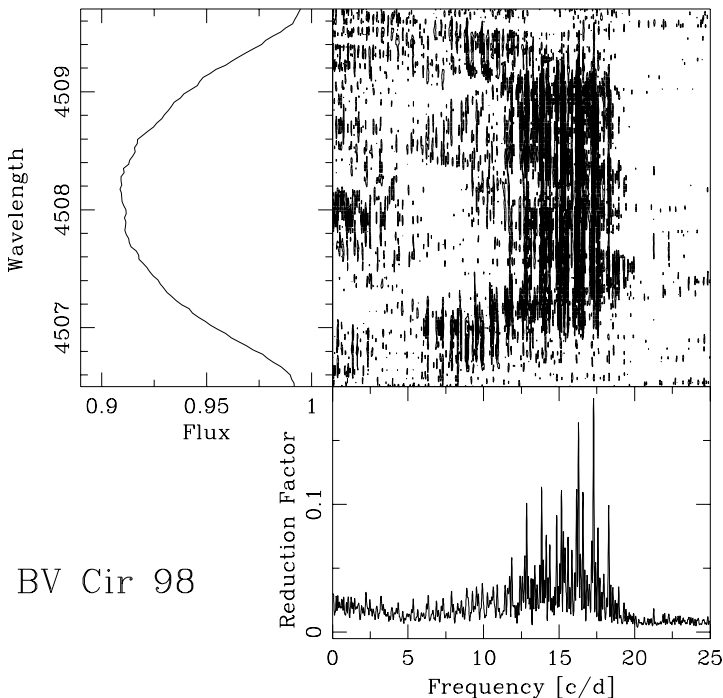


Figure 6. Frequency analysis of the variations in the profile of the FeII 4508 Å line of the star BV Cir. Left panel: Average profile. Central panel: pixel-by-pixel least-squares power spectra without known constituents (see text). Bottom panel “global” least-squares power spectrum (see text).

spectra computed with the least-squares technique without known constituents (i.e., the spectrum contains all signals present in the line variations, for details see below), and the lower panel shows the global least-squares spectrum (which is equivalent to a weighted average of the individual pixel-by-pixel spectra). In this case we are in the presence of rather complicated LPV which contain several modes with low, medium and high frequencies in the observer’s reference frame⁴. Since the data were obtained in a single site campaign the peak of each mode is flanked by rather strong 1 cd^{-1} aliases, and this, coupled with the intrinsic complexity of the pulsation spectrum, explains why the computed power spectrum is so entangled. In order to have a clear picture of the true pulsation spectrum is necessary to detect one by one all the periodicities or to

⁴Because of stellar rotation a non-axisymmetric non-radial mode with an oscillation frequency ν_0 in a reference frame co-rotating with the star is seen from the observer as having a frequency $\nu = \nu_0 - m\Omega$, where m is the mode azimuthal order and Ω is the stellar rotational frequency.

analyze the data with the CLEAN algorithm. The result of the application of this technique is shown in Fig. 7. Other examples of the application of the CLEAN algorithm to the pixel-by-pixel analysis are in the papers by Bossi et al. (1998) and De Mey et al. (1998).

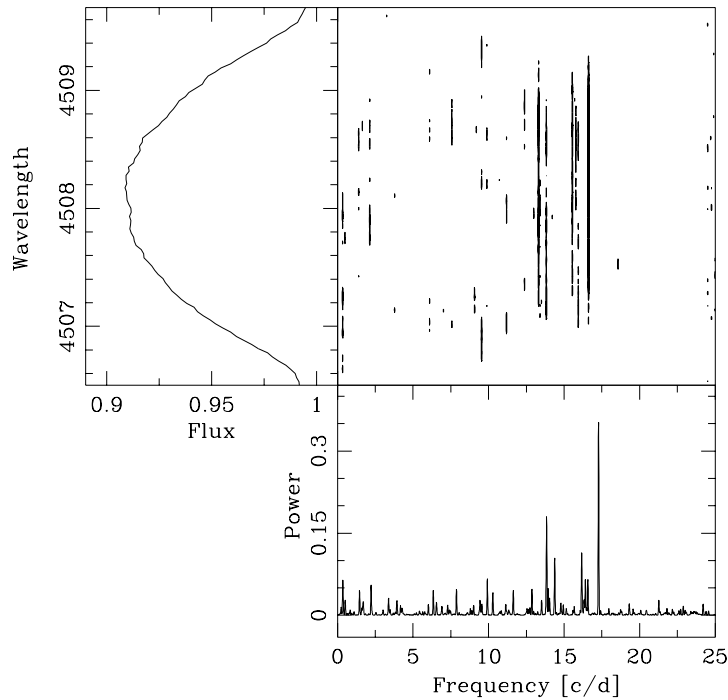


Figure 7. Frequency analysis of the variations in the profile of the FeII 4508Å line of the star BV Cir. Left panel: Average profile. Central panel pixel-by-pixel CLEAN power spectra. Bottom panel: average of the pixel-by-pixel CLEAN spectra.

The power spectrum of Fig. 7 is much more easily readable than that of Fig. 6 even if there are some aliases still present and probably in some cases aliases have been preferred to the true peaks. The reason is due to the fact that the CLEAN approach to select the peaks is completely automatic, and among other things it does not allow to select between competing aliases the use of the a priori knowledge, such as for example the fact that we know some correct periods from the light-curve analysis.

In our opinion and according to our experience, the most reliable approach for looking for multi-periodicities is to proceed to detect one by one the periods with the least squares technique. This approach has been slightly modified to best analyze LPV (Mantegazza & Poretti 1999) in order to define a “global” least-squares spectrum which includes the information of the variability of the whole profile.

The least-squares algorithm generalized to study LPV In general our data consist of a set of profiles of a spectral line $P(\lambda_j, t_k)$ (j is the pixel number and t_k is the time of the k -th spectrogram) whose global variance can be defined as

$$\sigma_T = \sum_{j,k} w_k^2 [P(\lambda_j, t_k) - P_0(\lambda_j)]^2 \quad (1)$$

where $P_0(\lambda_j)$ is the time averaged profile and the w_k 's are the normalized weights derived from the S/N of the individual spectrograms.

The frequency analysis of the variations present in these profiles can be iteratively performed in the following way: if we have already detected m periodic sinusoidal components (“known constituents”) and we are looking for the $m + 1$, we explore the useful frequency range ($0 < \nu_i < \nu_{max} \text{ cd}^{-1}$) by fitting each pixel time series j with the series

$$p_{i,j}(t_k) = \bar{p}_i + \sum_{l=1,m} A_{i,j,l} \cos(2\pi\nu_l t_k + \phi_{i,j,l}) + A_{i,j,m+1} \cos(2\pi\nu_i t_k + \phi_{i,j,m+1}) \quad (2)$$

where $\bar{p}_i, A_{i,j,l}, \phi_{i,j,l}$ (with $1 \leq l \leq m + 1$) are the free parameters.

Then we compute the global reduction of variance defined as

$$RF_i = 1 - \sum_{j,k} w_k^2 (p_{i,j}(t_k) - P(\lambda_j, t_k))^2 / \sigma_m \quad (3)$$

where σ_m is the global residual variance after the fit of the line profile variations with the m “known constituents”. The frequency ν_i giving the highest RF (or one of its 1 cd^{-1} aliases if there is a better agreement with the photometrically detected modes) is then selected as the $m + 1$ -th known constituent and the procedure is iterated again.

The search ends when no dominant peaks are apparent in the last spectrum. On this point a more quantitative criterion should be developed such as the one adopted by Breger et al. (1995) to assess the physical reality of peaks detected from light-curve frequency analysis.

At the end of this procedure, after having detected M known constituents, we can perform a final fit of $P(\lambda_j, t_k)$ and derive the functions: $\bar{p}_M(\lambda_j)$ (i.e., the best estimate of the average line profile), $A_l(\lambda_j), \phi_l(\lambda_j)$ (with $1 < l < M$) and also their formal errors.

As an example we report in Fig. 8 the frequency analysis of the variations in the 4508\AA line of the star HD2724. Each panel contains a “global least-squares spectrum” computed by introducing the frequencies of the terms detected in the previous spectra as “known constituents”. Fig. 9 summarizes in the upper panel the pulsation spectrum as derived from the frequency analysis of the previous figure. In the lower panel we show the same spectrum as obtained using the CLEAN algorithm. In this case the two approaches supply the same mode detection (the only discrepancy is on the selection of the lowest frequency peak where there is an uncertainty of 1 c/d , but as we can see in panel 4 of Fig. 8, the difference between the two peaks is very marginal).

Fig. 10 shows the behaviors of amplitudes and phases across the 4508\AA line profile of the terms detected in the previous example (functions $A_l(\lambda_j), \phi_l(\lambda_j)$

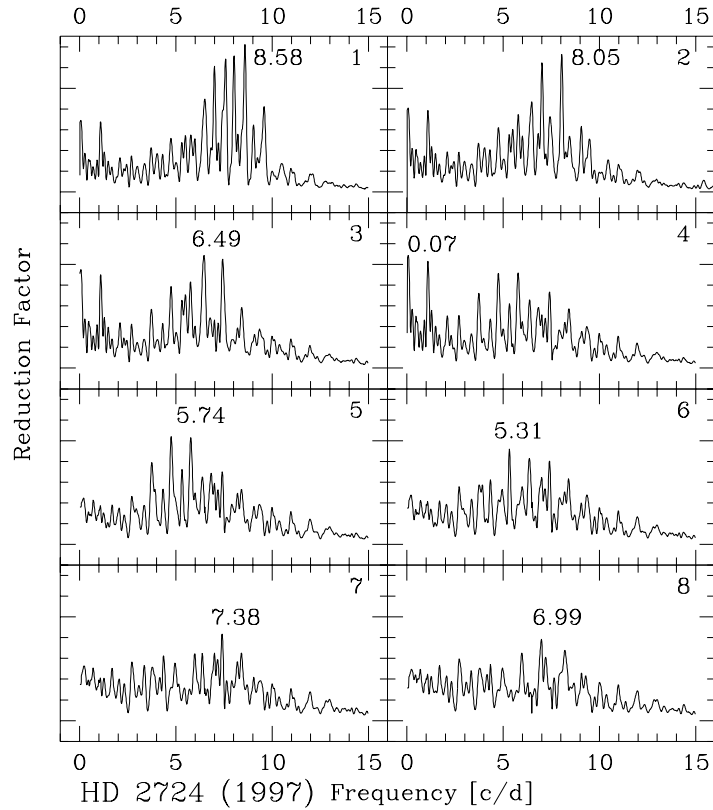


Figure 8. Complete frequency analysis with the global least-squares power spectra of the variations in the profile of the 4508\AA line of HD 2724 (1997 campaign). In each successive spectrum all the frequencies detected in the previous ones are given as “known constituents”. The order of computation follows the numbering reported on the upper left of each panel. In case of ambiguity between 1 c/d aliases the choice of the correct peak has been guided by the knowledge of the more accurate photometrically detected frequencies. The selected frequency at each step of the analysis is written beside the respective peak.

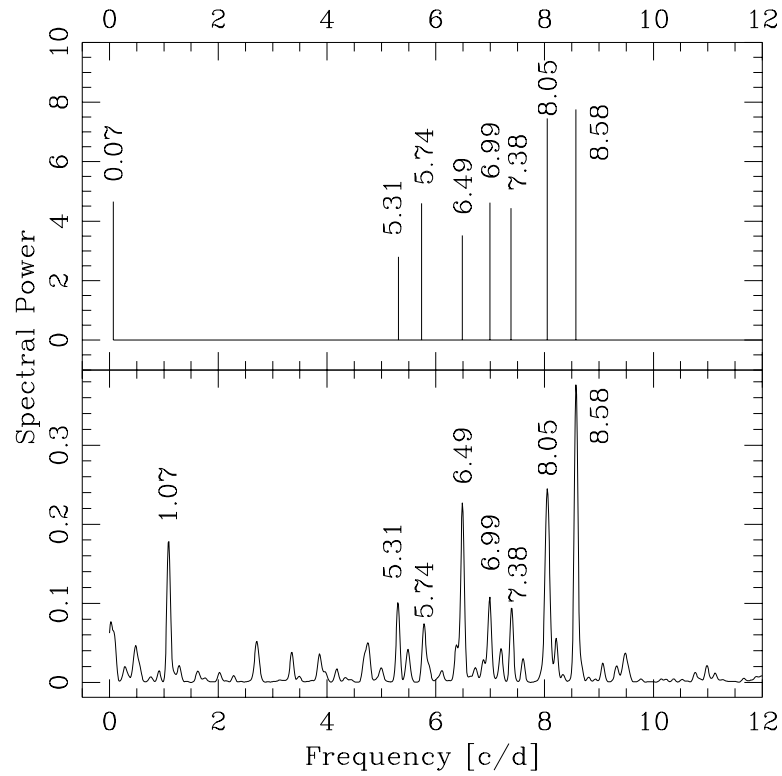


Figure 9. Upper panel: pulsation spectrum of HD 2724 as derived from the least-squares power spectrum analysis shown in the previous figure. In the ordinates the squared amplitudes averaged across the whole profile are shown. Lower panel: pixel-by-pixel CLEAN spectrum of the same data.

and their corresponding formal errors). The positions on the line profile are expressed in Doppler velocities as described in Section 2. The term at 0.07 cd^{-1} is not reported because it was probably introduced by an instrumental effect (see Mantegazza & Poretti 1999). It can be observed that the phase diagram of the 5.31 cd^{-1} term has the typical behavior of a low-degree retrograde mode (its phase increases in the same direction as the stellar rotation, i.e., with the wavelength). The opposite behavior is shown by the phases of the 8.58 cd^{-1} term, which is typical of a moderately high-degree prograde mode.

The diagrams that show the behavior of the phases of each mode across the line profile are very instructive to show the nature of the non-radial modes present in δ Scuti stars. In order to demonstrate this Fig. 11 shows a zoo of behaviors of such phases as we have derived them from our studies. Seven different modes are represented in the panels ranging from a high-degree retrograde mode (bottom panel) to a high-degree prograde mode and passing from an axisymmetric mode ($m = 0$, third panel from the bottom). For each panel we give the name of the star to which the mode belongs, the frequency of the mode in the observer's reference frame and its ℓ and m , as derived from the LPV fit technique described in the last section of this paper. The abscissae give the positions across the line profile with Doppler velocities (or equivalently wavelengths) increasing from left to right. $+1$ and -1 indicate a distance from the center corresponding to $+v \sin i$ and $-v \sin i$ respectively (i.e., in the Doppler map they correspond approximately to the limbs of the visible stellar disk).

4.2. The moment time-series analysis

The use of the line moments to study LPV was first introduced by Balona (1986a). Since the moments are also useful for mode identification, their definition is given in the paper by Aerts & Eyer (these proceedings). It suffices here to say that the zeroth order moment measures the equivalent width, while the first-order one the position of the line barycenter and hence it can be used as a measure of the stellar radial velocity. In his paper, Balona (1986a) gives some useful suggestions how to derive these quantities; to this end it is also useful to look at the paper by Balona et al. (1996). As an example Fig. 12 shows the behavior of the first three moments and of the zero-order one during one night of observations of the star X Cae (Mantegazza & Poretti 1996). Their variations are compared with the simultaneous variations in V light and $B - V$ color index. It can be observed that the first and third moment curves have a similar shape and are in anti-phase with respect to the light variations, while the second moment has a different behavior.

As in the case of the pixel-by-pixel time series the moment time series can be analyzed with the same techniques used to study light-curves. Since the moments are quantities integrated on the whole line profile, they are more sensitive to low degree modes, because the variations due to the high degree oscillations tend to be averaged out by the integration.

One interesting property of the moments is the fact that axisymmetric modes contribute with their fundamental frequency only to the variations of odd moments. Therefore the frequency analysis of the moment time series offers an easy way to detect these modes, and moreover, since often we face stars with a lot of excited modes, reducing the number of the modes affecting even moment

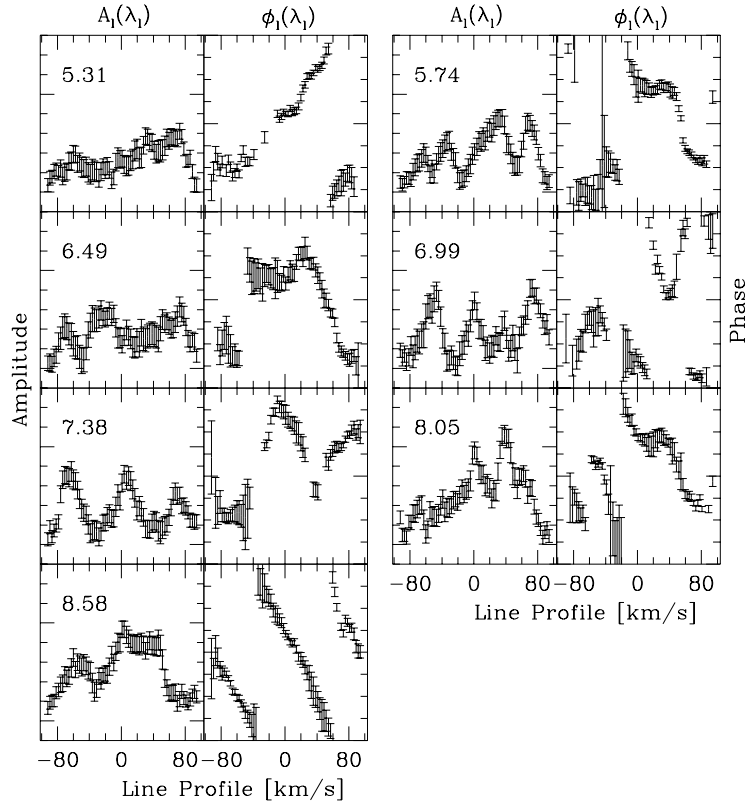


Figure 10. Behavior of amplitudes (first and third columns) and phases (second and fourth columns) across the profile of the 4508\AA line of the modes detected in the frequency analysis reported in Fig. 8 (functions $A_l(\lambda_j), \phi_l(\lambda_j)$ of the text). The bars are the formal errors derived as described in the text. All the diagrams have the same scale: amplitudes are in units of the continuum intensity (each tick corresponds to 0.001) and phases are in degrees (each tick corresponds to 50°). The ranges of the diagrams are from 0 to 0.008 and from -200° to $+200^\circ$ for amplitudes and phases, respectively. The frequency (in cd^{-1}) of each mode is reported at the upper left of the panel containing the respective amplitude function.

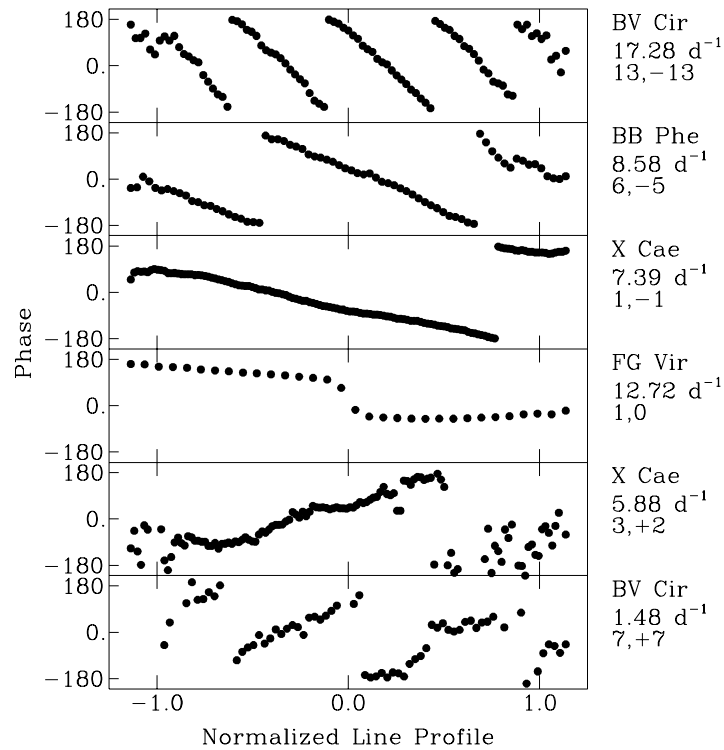


Figure 11. The zoo of non-radial modes present in δ Scuti stars as shown by the behavior of their phases across the line profile. We pass from high-degree retrograde modes (bottom panel) through axisymmetric modes ($m = 0$, third panel from bottom) to high-degree prograde modes. Beside each panel the name of the star to which the mode belongs is given together with its frequency in the observer’s reference frame and the proposed ℓ , m identification.

time series makes it easier to analyze them. As an example of this fact we show in Table 1 the results of the frequency analysis of the first 5 moments of FG Vir (1995 campaign, Mantegazza et al. in preparation). The detected frequencies in each moment time series are listed for each mode beside the well known and reliable values derived from light-curve analysis (Breger et al. 1998). Since the spectroscopic baseline is rather short (5 consecutive nights) and the campaign was single site, some 1 cd^{-1} aliases were picked up instead of the correct values. While up to 13 modes have been detected in the odd moments, the analysis of the even ones has allowed the detection of only two. According to what we said above it is evident that most of the modes should be axisymmetric. This is not surprising in view of the fact that the star is probably seen almost pole on, and therefore the detection of axisymmetric modes is favored by a selection effect.

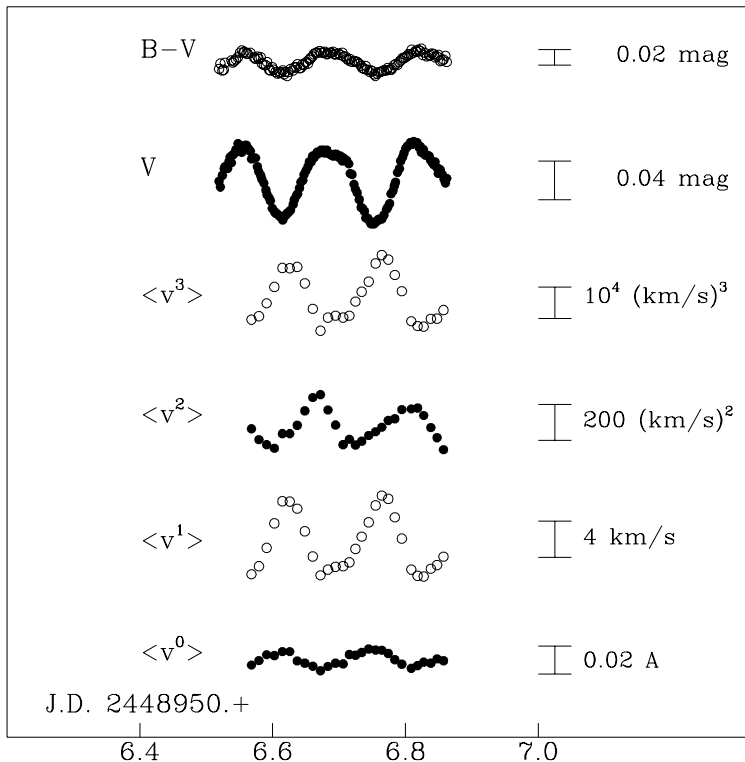


Figure 12. The variations of the first moments derived from the 4501, 4508 and 4515 Å lines are compared with the V and $B - V$ ones during one observing night of X Caeli. All the quantities, except V and $B - V$, increase toward the top.

4.3. Fourier Doppler Imaging (FDI)

This technique was first introduced to study LPV in δ Scuti stars by Kennelly et al. (1992) and successively developed and improved by Kennelly et al. (1998). A theoretical study of its properties has been performed by Hao (1998). This technique allows at the same time the detection of the modes producing LPV and the estimation of their non-radial degree (ℓ).

Because it is based on the computation of a two-dimensional Fourier Transform, which considers at the same time temporal and spatial variations, this technique is mainly sensitive to high-degree modes (see Kennelly et al. 1998, where these authors show also that the technique is more sensitive to odd azimuthal order modes than to even ones) and requires targets with rather high $v \sin i$'s.

For a description of it and an example of a two-dimensional Fourier amplitude spectrum see the paper by Aerts & Eyer (these proceedings, Fig. 8). One of the advantages of this method is that, by separating the detected modes both in temporal and spatial frequency, it allows, even if the temporal baseline is

Table 1. Frequencies of the terms detected from the analysis of the variations of the first five moments of FG Vir compared with the accurate frequencies detected from the light-curve analysis

$\langle v^1 \rangle$	$\langle v^2 \rangle$	$\langle v^3 \rangle$	$\langle v^4 \rangle$ cd ⁻¹	$\langle v^5 \rangle$	Photom.
10.17	9.17	9.21	9.19	8.19	9.199
9.65		9.66		9.60	9.656
11.16		12.13		12.03	12.154
12.72		12.72		12.73	12.716
17.11		17.01			16.074
19.92		19.92		19.91	19.868
21.07		21.07			21.052
21.32		20.30		21.28	20.288
20.53		20.55		20.60	21.551
23.43	22.47		22.46		23.403
23.17		23.17		23.19	24.200+24.228
34.14		33.17		34.16	34.119

not adequate, the resolution of modes with close temporal frequencies but very different spatial ones.

5. Recent campaigns

Tables 2 and 3 summarize the most recent spectroscopic campaigns on δ Scuti stars. In Table 2 we give for each star the epoch of the observations, the number of sites contributing to the campaign, whether or not there is simultaneous photometry, the adopted analysis technique and finally the reference. Table 3 gives more technical details such as the resolution, the spectral range, the average S/N of the individual spectrograms at the continuum level, the number of observing nights, the total useful observing time, the number of gathered spectra, the average exposure time and finally the lines (or their number if they were many) whose LPV were analyzed.

As we can see from Table 3 the observing parameters generally satisfy the requirements we derived in Section 3. We note moreover that moving from the oldest to the most recent campaigns their duration tends steadily to increase. This fact testifies that the observers became increasingly convinced that, given the complexity of the pulsation spectra, in order to get reliable mode detections baselines rivaling those of the photometric campaigns were necessary.

Fig. 13 shows the position of these objects in the color-magnitude diagram. We can see that they are rather uniformly distributed across the instability strip in the giant region. Main Sequence objects are generally missing because their fainter apparent magnitudes make it difficult to get spectrograms satisfying the observational constraints discussed in Section 3.

Table 2. Recent campaigns to study LPV in δ Scuti stars (FDI: Fourier Doppler Imaging; Mom: moment analysis; Pix: pixel-by-pixel analysis).

Star	Epoch	No. Sites	Simult. Photom.	Analysis Technique	Reference
τ Peg	Oct. 90	1	Yes	FDI	Kennelly et al. 1992
	Oct. 95	1	No	FDI	Kennelly et al. 1998
θ^2 Tau	Oct. 90	1	No	FDI	Kennelly & Walker 1996
	Dec. 92	4	No	FDI	Kennelly et al. 1996
FG Vir	Apr. 92	1	Yes	Mom	Mantegazza et al. 1994
	Apr. 95	1	Yes	Pix, Mom	Mantegazza et al. in preparation
X Cae	Nov. 92	1	Yes	Mom, FDI	Mantegazza & Poretti 1996
	Nov. 96	1	Yes	Pix	Mantegazza et al. 1999
ν UMa	Apr. 93	1	No	FDI	Korzennik et al. 1995
BB Phe	Sep. 93	1	Yes	Pix	Bossi et al. 1998
	Oct. 97	1	No	Pix	Mantegazza & Poretti 1999
HD 101158	Apr. 94	1	No	Pix	Mantegazza 1997
θ Tuc	Sep. 96	1	No	Pix, Mom	De Mey et al. 1998
BV Cir	Jun. 96	1	Yes	Pix	Mantegazza et al. in preparation
	Jun. 98	1	No	Pix	Mantegazza et al. in preparation
V480 Tau	Nov. 96	4	No	FDI	Hao et al. 1998
ϵ Cep	Sep. 97	3	No	FDI	Kennelly et al. 1999

Table 4 summarizes the number of periods detected in each of these stars according to the technique adopted to analyze LPV. For comparison in the same table the number of periods derived from the light-curve analysis are reported. The uncertain detections are given within brackets. The RV column reports the detection from the radial velocity variations, where here for radial velocities we mean those derived with techniques different from the first moment computation (for instance with correlation techniques). The results regarding V480 Tau are extremely preliminary (Hao, private communication) and many periods are expected to be found.

It is possible to see that in the cases where the temporal baseline is adequate the number of spectroscopic detections is comparable with those of photometric detections.

Some of the best spectroscopically studied objects have only few photometrically detected modes, because careful photometric campaigns have not yet been performed on these stars. A better coordination in the selection of the spectroscopic and photometric targets should be desirable in the future in order to get the most complete picture possible of the pulsation spectra.

Figures 14 and 15 show the best examples of pulsation spectra derived from spectroscopic analysis. For each star the projected rotational velocity is given below its name. The epoch of the observations is also given at the right of the star's names because, as we will show in the next subsection, the pulsation spectra can change considerably with the time. The heavy vertical segment at the top of each panel marks the expected position of the fundamental radial mode. In the case of θ Tuc this line is dashed, because it belongs to a binary

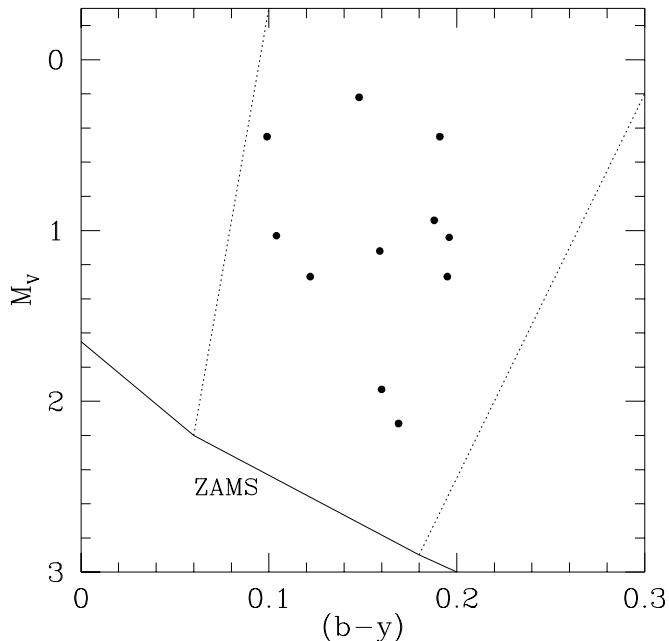


Figure 13. The targets of the most recent spectroscopic campaigns in the color-magnitude diagram. The dashed lines individuate the borders of the instability strip.

system, so the evaluation of its physical parameters is uncertain, and therefore the position of this line gives only the lower limit.

We see that in the cases of FG Vir, X Cae, BV Cir and τ Peg there are a few modes with frequencies in the observer’s reference frame below this value. In the cases of X Cae, τ Peg and for one of the modes of BV Cir these are retrograde p modes, which in the co-rotating reference frame have frequencies above the fundamental radial value. For the other two modes of BV Cir the question is open, because their identification is unclear, while the two modes of FG Vir could be g modes (Breger et al. 1999).

The amplitudes of the modes indicated with solid lines were derived from pixel-by-pixel analysis or from FDI and have been arbitrarily scaled for each star. The modes drawn with a dashed line for BB Phe, HD 101158, and θ_2 Tau were detected from the moment or the radial velocity analysis, and therefore their amplitudes cannot be compared with those of the others.

Several of the modes shown in these figures have not been photometrically detected. The number of modes with a spectroscopic detection only is indicated for each star in the last column of Table 4. We see therefore the complementarity between the two approaches and the need for both if we want to get the whole pulsation spectrum of the star.

The higher the projected rotational velocity is, the higher the number of purely spectroscopically detected modes is. This is an obvious selection effect, because high-degree modes can be detected only in fast rotators. This is con-

Table 4. Number of periods detected with the different spectroscopic techniques compared with the number of periods detected from light-curve analysis. The last column gives the number of modes detected from spectroscopic analysis but not seen in the photometric data

Star	Pix	FDI	Mom	RV	Photom.	Purely Spectr.
28 Aql			(2)	2	2	
k^2 Boo	1				1+(1)	
γ Boo	1				1	
τ Peg	31				1+(1)	29
θ^2		7		5	8	6
FG Vir	13				24+(8)	
X Cae	14	13		17		
v UMa		3			1	
BB Phe	8		10+(2)		10	3
HD 101158	2+(3)		1+(2)		3	
θ Tuc	4		4		10	3
BV Cir	14				9	7
V480 Tau		1+....			1	
ϵ Cep		~ 42			2+(1)	

firmed by the fact that, for instance, for a slow rotator such as FG Vir all the spectroscopically detected modes also have a photometric detection.

In order to get an idea of how the pulsation spectrum of a fast rotating δ Scuti star should appear as seen in the co-rotating reference frame, the observed frequencies of the modes detected and identified by Kennelly et al. (1998) with the FDI in τ Peg have been corrected for the rotational effect assuming that all of them were sectoral. The result is shown in the lower panel of Fig. 16. For comparison the upper panel shows the pulsation spectrum in the observer's reference frame and the dashed line shows the estimated position of the fundamental radial mode. We can see that in the co-rotating frame all the modes are clumped in the vicinity of the fundamental radial mode. The fact that a few of them have frequencies slightly lower than that of the fundamental radial one is probably due to the assumption that all the modes are sectoral, which probably for some modes is not true, and consequently their frequencies have been over-corrected toward low values.

5.1. Amplitude variations

As we can see from Table 2, there are a few stars for which observations have been performed in two campaigns. The best cases are those of X Cae, BB Phe and BV Cir. The availability of two independent datasets is very useful because it allows: a) the check of the reality of the modes which have not independently been detected from photometry, b) the detection of variations in the mode amplitudes. For the above-quoted three stars most of the modes have been independently detected in the two data sets and hence we are quite confident about their reliability.

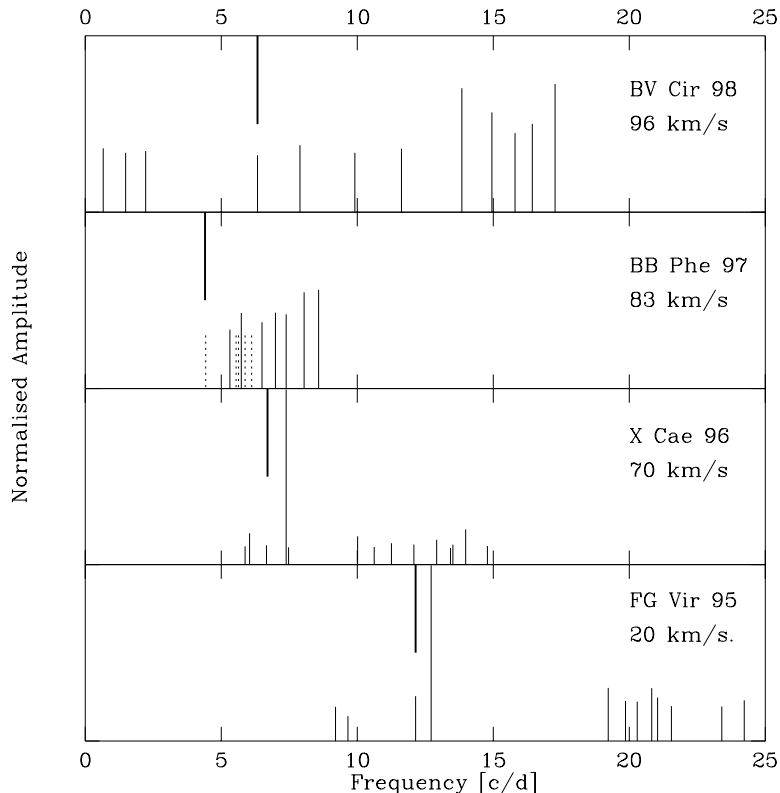


Figure 14. The pulsation spectra in the observer’s reference frame as derived from spectroscopic observations of the best studied δ Scuti stars. Solid lines: modes detected from pixel-by-pixel analysis or FDI. Dashed lines: modes detected from the line moment analysis. Heavy lines from the top: estimated position of the fundamental radial mode. For each star its projected rotational velocity and the year of the observations are reported .

In the cases of BB Phe and BV Cir there are large variations in the mode amplitudes. For both stars the strongest spectroscopic mode was different in the two seasons.

Figure 15 shows the global least squares power spectra without known constituents of BV Cir for the two campaigns. We clearly see the different frequency content: in the 1996 data the strongest peak is at 13.85 cd^{-1} , while in the 1998 data, even if this peak is still present, the highest one is at 17.28 cd^{-1} . This last peak in 1996 was below the detectability level. Comparing the two spectra we can also easily perceive their different frequency resolution due to the different temporal baselines (6 and 12 days, respectively).

Figure 18 compares the pulsation spectrum, as derived from the least-squares power spectrum analysis, of the two seasons. Seven terms are in common, but others are present only in one of the two datasets, in particular

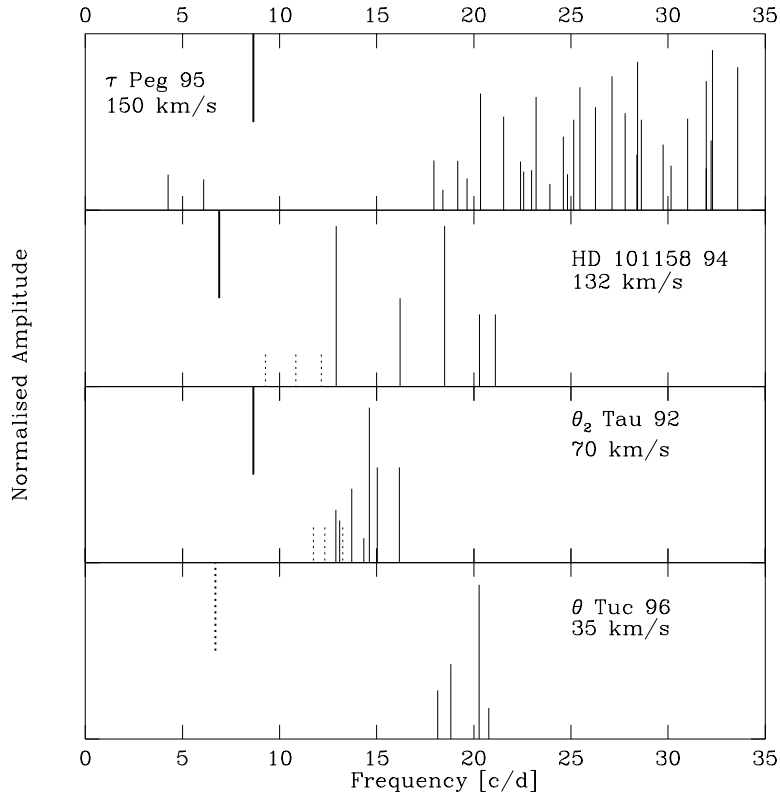


Figure 15. The same as the previous figure

the three highest frequency terms present in 1998, and which are among the strongest, were not detectable in the 1995 data.

Korzennik et al. (1995) on the basis of their FDI analysis of LPV in v UMa claimed that there were strong variations in the mode amplitudes from night to night. In this case it is easy to demonstrate that the more plausible explanation is that this is due to beats between unresolved modes: analyzing the data on a night by night basis, where the observations in each night covered between 2.5 to 5 hours only, the frequency resolution was extremely poor (between 5 to 10 cd^{-1}), hence the expected density of the pulsation spectrum amply allows the presence of these beats!

6. Mode identification by LPV fit in multiperiodic stars

In the paper by Aerts & Eyer (these proceedings) it is stated that the best approach to the mode identification is given by the direct fit of LPV, but unfortunately, according to them, this is possible for mono-periodic pulsators only. Recently, we (Bossi et al. 1998, Mantegazza & Poretti 1999, Mantegazza et al. 1999) have developed a technique that allows the fit of LPV for multiperiodic pulsators and moreover, if simultaneous spectroscopic and photometric obser-

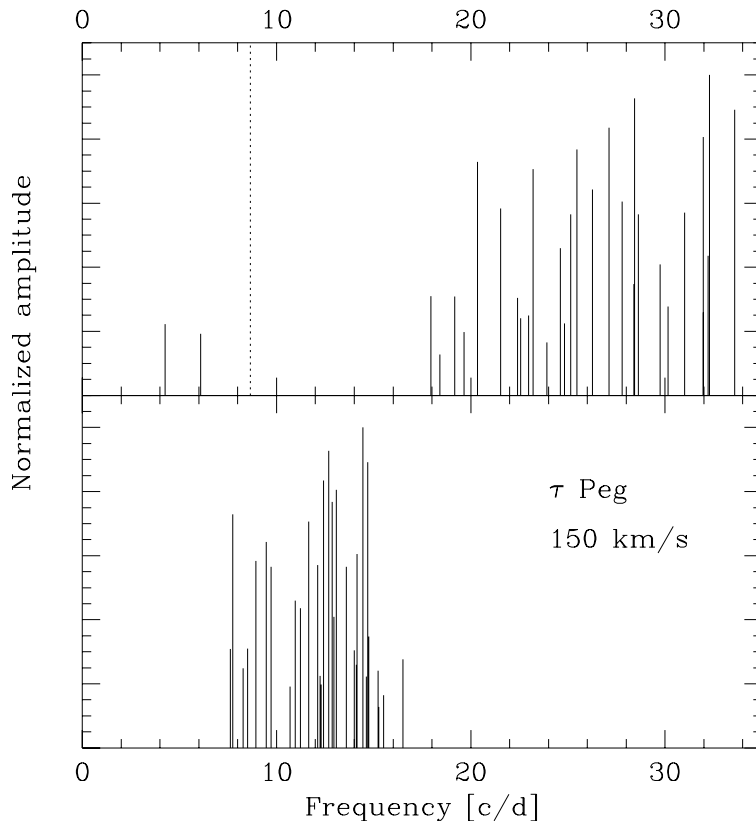


Figure 16. Upper panel: pulsation spectrum of τ Peg in the observer's reference frame; dashed line: estimated position of the fundamental radial mode. Lower panel: pulsation spectrum of τ Peg in the co-rotating reference frame, assuming that all the identified modes are sectoral.

variations are available, the technique can proceed to the mode identification by simultaneously fitting both variations.

In the presence of several simultaneously excited modes it is necessary to separate the contributions of each mode to the overall LPV and light variations.

To do this we approximate the perturbations $\Delta p_j(\lambda, t)$ induced by mode j on the line profile as:

$$\Delta p_j(\lambda, t) = \sum_i A_{ij}(\lambda) \cos(2\pi i \nu_{jt} + \phi_{ij}(\lambda)) \quad (4)$$

where the sum is on the Fourier harmonics of the j -mode. We can also estimate the formal errors on $\Delta p_j(\lambda, t)$ ($\delta \Delta p_j(\lambda, t)$) from error propagation by $\delta A_{ij}(\lambda)$ and $\delta \phi_{ij}(\lambda)$. These last quantities as well as $A_{ij}(\lambda)$ and $\phi_{ij}(\lambda)$ have been derived in Section 5.1 by simultaneously fitting all the detected modes and their harmonics to the observed LPV. Usually with a S/N of a few hundreds only the fundamental harmonic of each mode is easily detectable. Only for rather strong

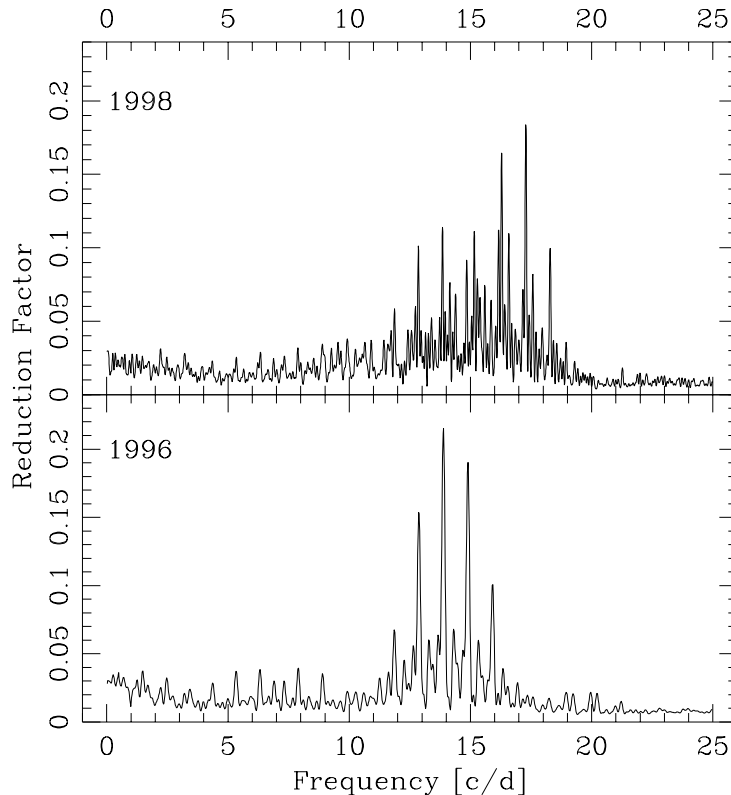


Figure 17. Global least-squares power spectra without known constituents of BV Cir in the two spectroscopic campaigns. It can be easily perceived how the frequency content has changed.

modes, such as for the dominant mode of X Cae (Mantegazza et al. 1999), the first harmonic is also detectable.

Fig. 20 shows for instance the amplitude (right panels, dashed lines) and phase (left panels, dots) variations across the 4501 Å line profile of X Cae derived from this simultaneous least-squares fit of the fundamental frequency (upper panels) of the dominant mode and its first harmonic (lower panels). The reconstructed LPV (equation 4) due to this mode are shown as solid lines in Fig. 19. In this case the functions $\Delta p_j(\lambda, t)$ have been computed for ten equispaced phases of a complete cycle.

We can try to fit the functions $\Delta p_j(\lambda, t)$ (eq. 4) with perturbations computed with a model of a non-radial pulsating star viewed at a certain inclination i . So for each plausible choice of ℓ, m, i we can build a discriminant

$$\sigma_p(\ell, m, i) = \sum_{\lambda} \sum_t \frac{(\Delta p_j(\lambda, t) - \Delta p_c(\lambda, t, \ell, m, i))^2}{\delta \Delta p_j(\lambda, t)^2} \quad (5)$$

where $\Delta p_c(\lambda, t, \ell, m, i)$ are the computed profile variations which best fit the observed ones.

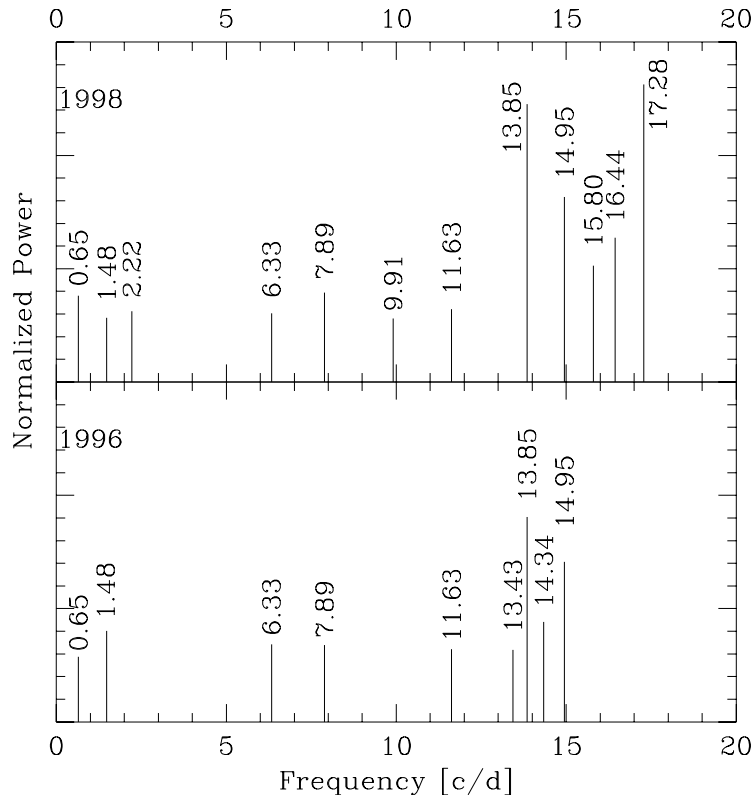


Figure 18. Comparison between the pulsation spectra of BV Cir derived from LPV in 1996 and in 1998.

Moreover, if we have simultaneous photometric observations, we can obtain, by simultaneously fitting all the terms detected in the light curve, amplitude and phase with respective errors for the j mode. Therefore we can calculate its light variations and relative errors ($l_j(t)$ and $\delta l_j(t)$) and compare them with those predicted by the best fitting models and obtain the discriminant:

$$\sigma_l(\ell, m, i) = \sum_t (l_j(t) - l_c(t, \ell, m, i))^2 / \delta l_j(t)^2. \quad (6)$$

A global discriminant is then defined as:

$$\sigma_T(\ell, m, i) = \sigma_p(\ell, m, i) + \sigma_l(\ell, m, i). \quad (7)$$

This is the function which is minimized with a non-linear least-squares fit for each detected j mode and for any choice of ℓ, m, i .

The model we used to compute the synthetic line profile variations $\Delta p_c(\lambda, t, \ell, m, i)$ and light variations $l_c(t, \ell, m, i)$ is the one described by Balona (1987). For each assigned ℓ, m, i the computed profile variations can be modeled according to the amplitude and phase of vertical (v_r) and horizontal (v_h) velocities and flux variations. For δ Scuti stars usually $v_h \ll v_r$ and therefore in order

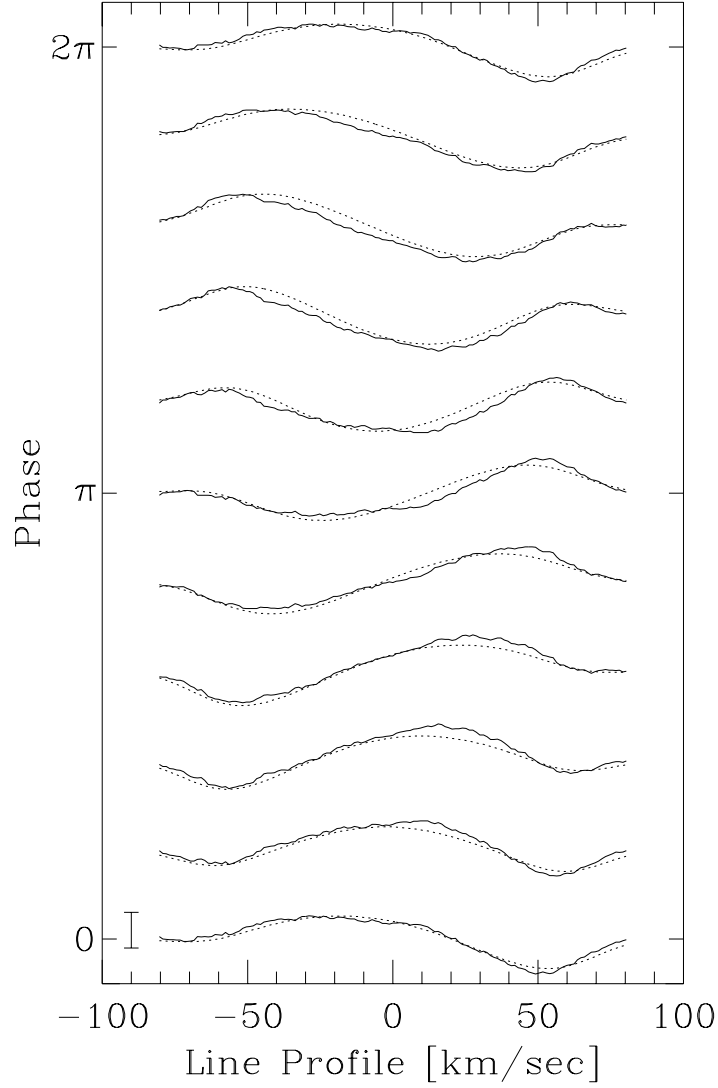


Figure 19. The variations induced on the profile of the TiII 4501Å line of X Cae by the dominant mode (7.39 cd^{-1}) phase over one cycle (solid line) and the best fitting model of the mode which gives the least global discriminant ($\ell = 1$, $m = -1$, and $i = 70^\circ$, dashed lines). The small bar at the lower left indicates an amplitude of 0.02 in continuum intensity units.

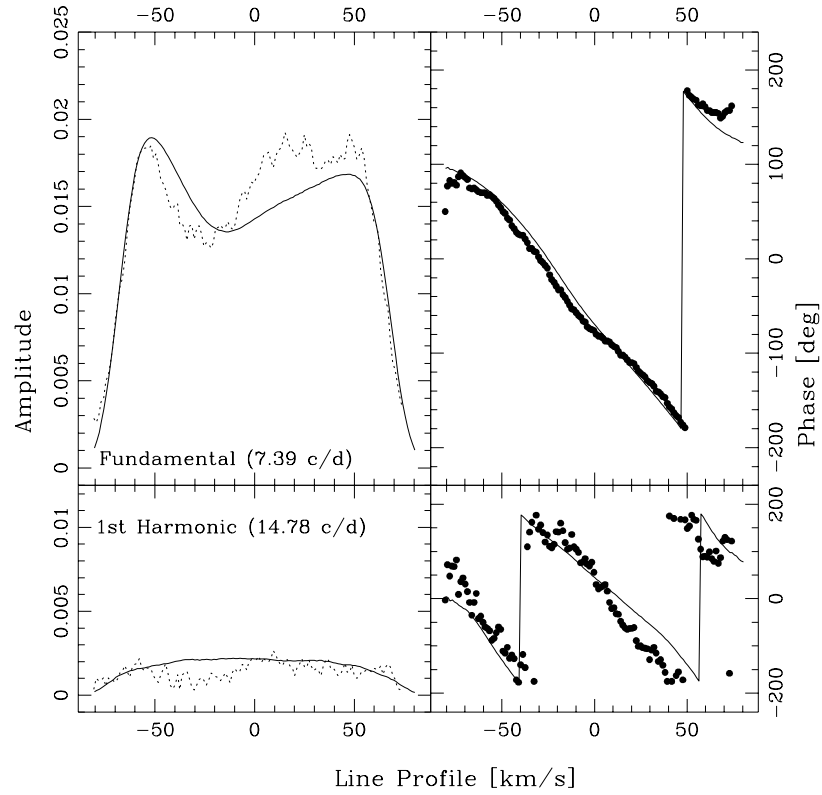


Figure 20. The behavior across the profile of the 4501\AA line of X Cae of the model which best fit the variations induced by the dominant mode ($\ell = 1$, $m = -1$ and $i = 70^\circ$) is compared with the same quantities as derived from the observations. The top panels refer to the fundamental harmonic while the bottom one to the first harmonic. The amplitudes (in continuum units) are shown on the left; the phases on the right.

not to introduce into the model too many free parameters, we keep the usual theoretical relation (e.g., Heynderickx et al. 1994) $v_h = 74.4Q^2v_r$ (Q pulsation constant) and $\psi_h = \psi_r$.

The observed light variations constrain strongly the computed flux variations, so it is very useful to have simultaneous spectroscopic and photometric data, otherwise in order to get meaningful physical results it is better to fit a simplified model which considers velocity variations only, neglecting flux variations.

By applying this approach to fit the reconstructed profile and light variations due to the dominant mode of X Cae (solid lines of Fig. 17) we found that the least global discriminant is supplied by a non-radial mode with $\ell = 1$, $m = -1$, and $i = 70^\circ$. This result is in agreement with that derived from the independent dataset of the previous (1992) observing season (Mantegazza & Poretti 1998), and which was obtained from the moment variation fits with the technique developed by Balona (1987) (see also Balona et al. 1996), and which is different from the approach with the moments described in Aerts & Eyser (these proceedings).

The LPV computed according to this model are represented as dashed lines in Fig. 19 and explains the 94% of the variance. The same model fits the observed B variations due to this mode with a standard deviation of 0.4 mmag.

Finally from the computed LPV we can also derive the behavior of amplitude and phase across the line profile both for the fundamental and first harmonic terms. These functions are represented as solid lines in the panels of Fig. 20.

6.1. Improved estimate of $v \sin i$ and W_i

As we have said in Section 2, the average line profile tends to be wider than the nonpulsation one and consequently there is the risk that both the projected rotational velocity and the intrinsic line width can be overestimated. A better way to estimate these two quantities is to give them as two more free parameters in the model which is non-linearly fit to LPV. For instance in the case of X Cae from the 4501Å line we get $v \sin i=69.0$ km/s and $W_i= 11.9$ km/s from the average line profile, while the non-linear LPV fit with the best-fitting mode ($\ell = 1$, $m = -1$) for the 7.39 cd^{-1} mode supplies $v \sin i=68.6$ km/s and $W_i=7.7$ km/s. While the estimate of the projected rotational velocity has not appreciably changed, the intrinsic line width has been considerably decreased.

7. Conclusions

In this paper we have presented the main observational characteristics of LPV in δ Scuti stars, and we have discussed how they can be observed and which techniques can be adopted to detect the pulsation modes. Moreover, a review of the main results obtained from the application of these techniques has been given. As we have seen, the number of stars carefully studied is at the moment scanty, so it is difficult to draw very general conclusions, although some facts, which can be useful as guidelines for future studies, can be pointed out:

- The careful observation and analysis of LPV allows several pulsation modes to be detected. If data with adequate S/N and temporal baselines are available the number of spectroscopically detected periods rivals the number which are photometrically detected.

Many of these detections are purely spectroscopic, especially for stars with high $v \sin i$: photometric observations alone are not sufficient to get the complete pulsation spectrum.

- The variability of the mode amplitudes is quite common. Sometimes some modes have amplitudes below the detectability threshold. Again, to get the complete pulsation spectrum, we need to observe the star at different epochs, and it may be desirable to get higher S/N data in order to better monitor the evolution of the amplitudes.
- Period detections can be rather reliable: several of the spectroscopically detected modes have also been photometrically detected and moreover, for the stars with two spectroscopic campaigns, many of the periods have been independently detected in both datasets. Again, to do a good job, we need high S/N with long baselines.
- The three different analysis techniques presented in Section 4 tend to be complementary: the moment method is particularly suited for low-degree modes; FDI works preferably on high-degree ones and on stars with high $v \sin i$; the pixel-by-pixel analysis works both on low- and high-degree modes, and, for the detection of the low-degree ones, it is preferable to study stars with low $v \sin i$. For instance, with this technique we were able to detect several modes in FG Vir, which has a $v \sin i$ of only 20 km/s.
- Given the complexity of the pulsation spectra, in order to get adequate frequency resolution and to avoid aliasing ambiguities, we need relatively long baselines (possibly comparable to the photometric ones) as well as multi-site campaigns.
- We have already pointed out the need for data with good S/N . Given the very small amplitudes of most of the modes (a few thousandths of the continuum intensity), in order not to merely detect them, but also to proceed to their identification, a S/N better than 500 is desirable.
- Since together with high S/N data we also need high spectral and temporal resolutions and short exposure times (unless large telescopes are used for extended periods of time, which is almost a hopeless possibility), it is important to develop and to adopt techniques that add the information from many spectral lines. This would entail the use of medium size telescopes, which are more accessible. Much work is still to be done in this direction, especially if the added information is used not merely for mode detection but for identification, too.
- As an immediate consequence of the previous items, it is evident that the best strategy to get a complete picture of the pulsation behavior of a δ Scuti star is to observe it simultaneously both photometrically and spectroscopically for several seasons and in the context of multi-site campaigns.

In this respect the few researchers active in the field should coordinate their efforts in order to study a few carefully selected targets.

Finally in the last part of this paper an approach to mode detection by LPV fitting in multiperiodic variables has been presented. This approach at the moment is not free of problems; for example, a better model of the LPV to fit to the data is needed, a model that at the same time is not too cumbersome, because the routine which uses it is called thousands of times during the minimization procedure. Another problem is the same one faced by the moment method described by Aerts & Eyser (this proceedings), i.e., the lack of confidence intervals for the minima of the discriminant, which makes it difficult to compare the competing modes. This second problem could be rather easily overcome once the first has been successfully addressed and the errors on the reconstruction of the LPV produced by each mode correctly estimated, because the discriminants (eqs. 5–7) have a χ^2 shape and therefore their statistical properties are well known.

Acknowledgments. I am grateful to E. Poretti for a critical reading of the manuscript and to M. Bossi for some fruitful discussions.

References

- Balona, L.A. 1986a, MNRAS, 219, 111
 Balona, L.A. 1986b, MNRAS, 220, 647
 Balona, L.A. 1987, MNRAS, 224, 41
 Balona, L.A. et al. 1996, MNRAS, 281, 1315
 Bossi, M., Mantegazza, L., & Nuñez, N.S. 1998, A&A, 336, 518
 Breger, M. 1979, PASP, 91, 5
 Breger, M. et al. 1995, A&A, 297, 483
 Breger, M. et al. 1998, A&A, 331, 271
 Breger, M. et al. 1999, A&A, 341, 151
 Campos, A.J., & Smith, M.A. 1980, ApJ, 238, 667
 De Mey, K., Daems, K., Sterken, C. 1998, A&A, 336, 327
 Hao, J. 1998, ApJ, 500, 440
 Hao, J., et al. 1998, Proc. of the ESO Workshop, Cyclical Variability in Stellar Winds, L. Kaper & A.W. Fullerton (Berlin: Springer-Verlag), 380
 Heynderickx, D., Waelkens, C., Smeyers, P. 1994, A&A, 105, 447
 Kennelly, E.J., Walker, G.A.H., & Hubeny, I. 1991, PASP, 103, 1250
 Kennelly, E.J., & Walker, G.A.H. 1996, PASP, 108, 327
 Kennelly, E.J. et al. 1992, PASP, 104, 15
 Kennelly, E.J. et al. 1996, A&A, 313, 571
 Kennelly, E.J. et al. 1998, ApJ, 495, 440
 Kennelly et al. 1999, in ASP Conf. Ser. 185, Precise stellar radial velocities, ed. J.B.Hearnshaw & C.D.Scarfe, (San Francisco: ASP), 264
 Korzennik, S.G., et al. 1995, ApJ, 443, L25

- Mantegazza, L. 1997, *A&A*, 323, 845
Mantegazza, L., & Poretti, E. 1996, *A&A*, 312, 855
Mantegazza, L., & Poretti, E. 1998, in *IAU Symp. 181, Poster Vol.* (Université de Nice), 267
Mantegazza, L., & Poretti, E. 1999, *A&A*, 348, 139
Mantegazza, L., Poretti, E., & Bossi, M. 1994, *A&A*, 287, 95
Mantegazza, L., Zerbi, F.M., & Sacchi, A. 2000, *A&A* in press
Roberts, D.H., Lehar, J., Dreher, J.W. 1987, *AJ*, 93, 698
Smith, M.A. 1982 *ApJ*, 254, 242
Struve, O. 1950, *PASP*, 1953, 252
Vaniček, P. 1971, *Ap&SS*, 12, 10
Vogt, S.S., & Penrod, G.D. 1983, *ApJ*, 496, 127
Walker, G.A.H., Yang, S., Fahlman, G.G. 1986, *ApJ*, 320, L139
Wright, W.H. 1900, *ApJ*, 12, 256
Yang, S., & Walker, G.A.H. 1986, *PASP*, 98, 1856